NAIC-ID(RS)T-0528-96

NATIONAL AIR INTELLIGENCE CENTER

SELECTED ARTICLES

Approved for public release: distribution unlimited

HUMAN TRANSLATION

NAIC-ID(RS)T-0528-96 22 January 1997

MICROFICHE NR:

SELECTED ARTICLES

English pages: 32

Source: Unknown

Country of origin: China
Translated by: Leo Kanner Associates
F33657-88-D-2188
Requester: NAIC/TATD/Bruce Armstrong
Approved for public release: distribution unlimited.

TABLE OF CONTENTS

GRAPHICS DISCLAIMER

All figures, graphics, tables, equations, etc. merged into this translation were extracted from the best quality copy available.

EFFECT OF WORKING GASES IN CO_2 LASER ON OUTPUT

Hu Xiyuan, Xiong Jiangang, Hu Lunji,
Chen Zutao, and Luo Hong
Huazhong University of Science and Technology

ABSTRACT: The decrease in the output power of a high power CO_2 laser with transverse gas flow system after long time service was investigated. It is shown that, with an adjustment on working gases in a CO_2 laser, the output power can be compensated for. It was proved in practice that the method of adjusting working gases can effectively improve the service life of the high power CO_2 laser.
KEY WORDS: CO_2 laser, working gases, output power.

High power CO_2 lasers with a transverse gas flow system are prominent in laser processing in China. Having been operated for 10 or more years, some of these laser devices are facing a critical problem of a fall-off in output power

After nearly ten years' study of a 2kW CO_2 laser with a transverse gas flow system, we determined some regularities of the total pressure and gas-distributing ratio of working gases, and the output power and the adjusted parameters of this laser device during long-term operation. Through these efforts, we obtained fairly complete gas distribution data that are suitable

for such long-term operation of high power CO_2 laser devices with a transverse gas flow system; the data are helpful in increasing laser device operating life and prolonging their operating periods between overhauls.

Structure and Technical Specifications of Laser Device

1. Basic Structure of Laser Device

The HGL-81 electrically excited CO_2 laser device with a transverse gas flow system that we used is an early model. It is a semi-closed laser, in which working gases rapidly flowed in a transverse direction under high pressure.

The discharge mode of this laser consisted of high-pressure direct-current glow discharges with a glow-initiating voltage 2600-3000V, a working voltage 3100-3700V, and a maximum working current<6A. The electrodes were in the "needle-plate" form. The anode consisted of a water cooling copper plate and an input electrode, while the cathode was made up of part of a high-pressure insulating plate and tungsten needles mounted on the plate; there were three rows of tungsten needles aligned along the optical axis with each row, respectively, containing 100 needles.

The flow direction of the working gases, the discharge direction, and the direction of the optical axis are three axes in quadrature, as shown in Fig. 1. The working gases wee a mixture of CO_2 gas, N_2 gas, and He gas, driven by a 15,000rpm axial flow gas compressor. These gases flowed at a rate of 50m/sec when passing through the discharge zone.

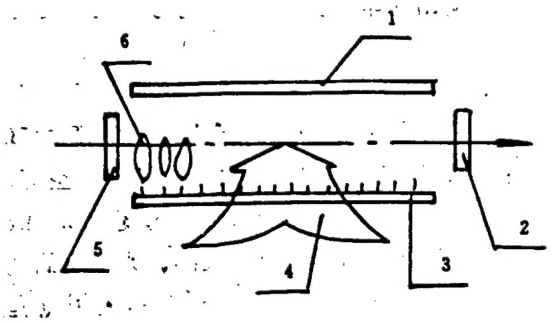

Fig. 1.

KEY:: 1 - anode 2 - output window
3 - cathode 4 - gas inlet
5 - total reflector 6 - discharge flow

A JZS-2F10 cold-water unit provided cold water at 8-10^{0}C, which, passing through a heat-retaining water tank, a pump and a laser, performed closed-circuit circular cooling.

2. Major Technical Indicators of the Laser Device

This laser was a high power continuous output CO_2 laser with a transverse gas flow system, which features the following major technical indicators:

Output power: maximum laser output power is 2.0kW

Laser wavelength and pattern: λ=10.6μm, multimode

Beam diameter: Φ30mm

Far-field divergence angle: <3mrad

Instability of output power: ≤±5%

Photoelectric conversion efficiency: >13%

Component-distribution ratio of working gases: CO_2:N_2:He=1:7:20

Total pressure of working gases: >1.2 X 10^{4}Pa

Operation and Detection Methods

1. Operation of Laser Device

This laser device was continuously operated for ten years. It operated for over 400 hours per year and cumulatively, it accrued nearly 5000 hours. During this time, there was no overhaul except for a portion of the output window and part of the current-limiting resistance being replaced, while the optical path system, anode plates, and cathode needles in the laser wereintact.

At present, this laser still can maintain a laser output power of 1.8-2.0kW, and can be continuously run for 8h during each gas distribution.

2. Detection Instruments and Methods for Gas-distribution System

This laser device was evacuated with a 2x-30A leaf-rotating vacuum pump, and its vacuum level was determined with a WZR-1P thermal couple vacuum gauge. In addition, the distribution ratio and filling of working gases were determined with an 0.5 precision YG cursor micromanometer. For accurate reading of low gas pressure values, a micromanometer with a range 0-4kPa was used in determining the CO_2 gas distribution and filling; a micromanometer with a range of 0-40kPa served in measuring the distributed and filled gas when its pressure increased. With these means, the CO_2 gas distribution and filling can reach a precision at the 10^{-1} level.

To monitor the variation in working temperature of the working gases in the discharge zone, a TH-80 interchangeable semiconductor point thermometer was installed, respectively, at the gas inlet and outlet in the discharge zone, with gas sampling for comparison. Since the temperature of working gases at the inlet was lower, the range selected was $0-50^0C$, while at the

outlet it was 0-100^{0}C.

Results of Long-term Operation and Analysis

1. Regularities of Laser Output Power Variation

In long-term operation of the laser device, the laser output power varied remarkably with its accrued operating time as shown in Fig. 2. When input power was constant, the laser output power gradually decreased in a stepwise manner with increase in operating time. In other words, the output power of the high power CO_2 laser device with a transverse gas flow system decreased gradually in stages.

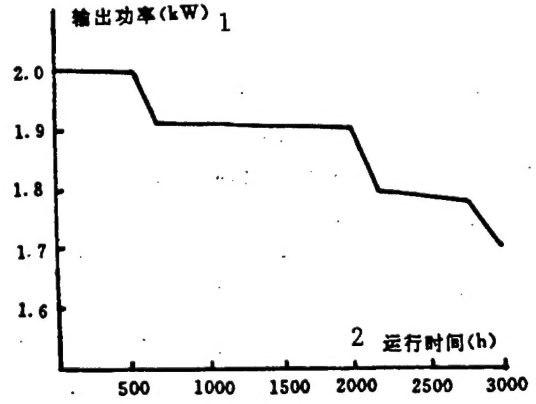

Fig. 2. Relationship between laser output power and operating time
KEY: 1 - output power 2 - operating time

Once the output power of the laser device decreased, it can be compensated for only by increasing its input power, i.e., by increasing input voltage and current. However, the input power of the laser device cannot be increased indefinitely. Given this situation, we turned our attention to the total pressure and distribution ratio of the working gases.

2. Effect of Total Pressure of Working Gases

Under the precondition that the output power of the laser device remained within 2.0kW±5%, the working gases were distributed according to the technical requirements of the device during its initial operation, i.e., CO_2:N_2:He=1:7:20, the total gas pressure being 13332P_a. As the output power decreased, the total gas pressure should be gradually adjusted, the regularities of such adjustment being shown in Fig. 3. At constant input power of the laser device, selecting different total gas pressure values during different operation periods can make the high power CO_2 laser device with a transverse gas flow system maintain a higher photoelectric conversion efficiency and can provide maximum output power.

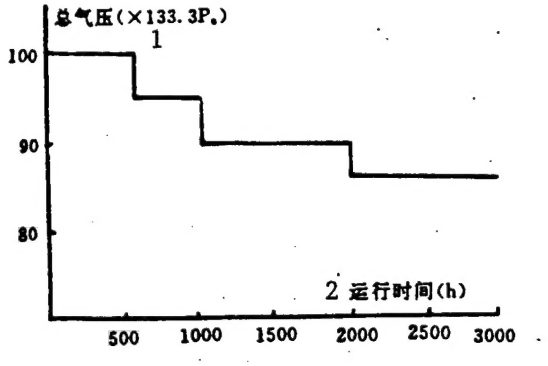

Fig. 3. Relationship between total gas pressure and operating time (to ensure output power 2.0kW)
Key: 1 - total gas pressure 2 - operating time

Additionally, following long-term operation, the cathode needles in the laser device will be scorched, and the cathode spray will give rise to contamination of anode plates and will increase discharge density. Under such circumstances, selecting high-pressure working gases will inevitably cause the input voltage to increase and even to exceed the safety standard for

the laser device.

Moreover, with different laser device operating times, the regularities of variation in the total pressure of working gases and the output power will vary, also as shown in Fig. 4. At a constant partial pressure distribution ratio of working gases, their total pressure and accordingly, the laser output power will increase when the laser has operated approximately 800 hours. Yet when the total pressure increases to 12.66kPa, it will no longer have a remarkable effect on output power.

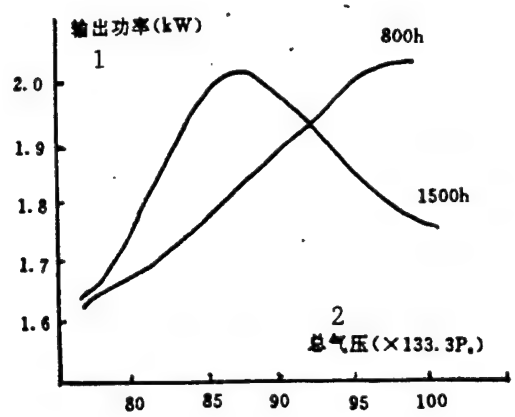

Fig. 4. Relationship between total gas pressure and output power during different operation periods
KEY: 1 - output power 2 - total gas pressure

Since the laser device operated for approximately 1500h, and total pressure of working gases was less than 11.5kPa, the output power will increase with increase in total gas pressure. But once the total gas pressure exceeds 11.7kPa, the output power will decrease with increase in total gas pressure.

To summarize, to ensure a long and steady maximum output power of the high power CO_2 laser device with a transverse gas flow system, total pressure of its working gases should be gradually lowered. Furthermore, it always has an optimal value

during different operating periods, which varies continually with the steadily increasing operating time of the laser device.

3. Relationship of Partial Pressure Ratio between CO_2 and N_2 Gases

In a high power CO_2 laser device with a transverse gas flow system, the process of CO_2 and N_2 energy transfer due to their collision is similar to resonant transfer:

$$N_2(V=1\sim4)+CO_2(00^0)\rightarrow N_2(V=0)+CO_2(00^0V_3=1\sim4)^{[1]}$$

These $CO_2(00^0V_3)$ levels will further transfer to the $CO_2(00^01)$ energy level through semi-level transition.

Properly selecting the CO_2/N_2 partial pressure ratio is vitally important for enhancing the laser device gain and output power. The relationship between this ratio and total pressure of working gases is shown in Fig. 5. It can be seen from the figure that this ratio increases with increase in laser device operating time, which indicates that with increase in device operating time, the electron impact excitation of CO_2 molecules will weaken, while the resonant transfer excitation will strengthen, resulting in an increase in N_2 gas partial pressure.

When the CO_2/N_2 partial pressure ratio increased, the total pressure of working gases definitely will decrease. Statistics based on years of experimentation show that with increase in N_2 gas content, the input voltage of the laser device will remarkably increase and, correspondingly, the photoelectric conversion efficiency will vary greatly, although the input current somewhat decreases, i.e., total output power remains basically unchanged. In this case, if total pressure of working gases does not decrease, input voltage will be excessive.

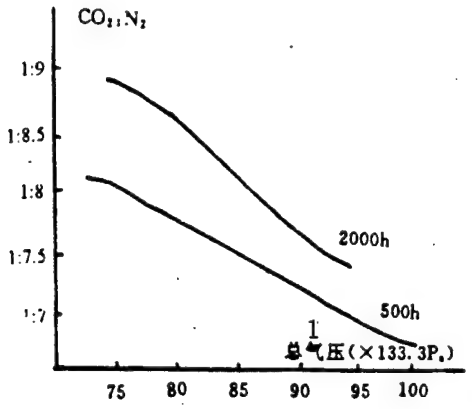

Fig. 5. Relationship between CO_2/N_2 partial pressure ratio and total gas pressure
KEY: 1 - total gas pressure

During different operating periods of the high power laser device with a transverse gas flow system, there is an optimal value of the CO_2/N_2 partial pressure ratio; and there is an optimal value, in turn, for the ratio of this ratio to total gas pressure. For example, when the laser device operated approximately 600 hours, $CO_2:N_2=1:7$, and the optimal total gas pressure value was 12.7kPa; when the laser operated approximately 1800 hours, $CO_2:N_2=1:7.6$, and the optimal total gas pressure value was 11.5kPa. As for other combinations of the partial pressure ratio and total gas pressure shown in Fig. 5, some of these combinations, though able to reach the maximum output power, do not allow a longer operating time during each gas filling, while other combinations may lead to a rapid temperature rise of working gases while operating.

The reason for the foregoing situation is that the increase in N_2 content can cause an increase in the rate of the 00^01 energy level that excites CO_2 molecules, but at the same time it can also cause a decrease in CO_2 molecular population. In addition, the increase in N_2 content tends to generate N_2O molecules in the gas discharge process, which can offset the

efficiency of the $00^0 1$ energy level in exciting CO_2 molecules[2]. All these factors may lead to a decrease in laser output power.

4. Effect of He Gas Partial Pressure Values

With a thermal conductivity one order of magnitude higher than for the CO_2 and N_2 gases, He gas can cause the temperature of working gases to decrease rapidly. Also, He can increase the relaxation rate of the $10^0 0$ level energy during irradiation of laser and thus, can decrease the population at that energy level and increase the CO_2 laser output power[2].

It can be concluded from experimental data that if the CO_2/N_2 partial pressure ratio is selected as 1:18-22, it has an indistinct effect on the laser device output power, but if the He proportion is excessively high, and accordingly, the total pressure of working gases is too high, the output power of the laser device still may decrease.

This can be attributed to the effect of the total pressure of working gases, since the increase in He partial pressure can lead to an increase in total gas pressure; or otherwise, changing the original proportion of N_2 partial pressure may cause a decrease in laser output power.

The He partial pressure ratio that was selected during initial operation still can be employed when the laser device was operated approximately 2000 hours without overhaul.

5. Temperature Variation Regularities of Working Gases

During operation of the high power CO_2 laser device with a transverse gas flow system, the temperature of working gases in the discharge zone should be vigorously restricted, because it has a direct effect on laser output power. The foregoing laser

device was subjected to closed-circuit circular cooling with cold water at 8-10^{0}C, provided by a JZS-2F10 cold-water unit. The whole process was under real-time monitoring at the inlet and outlet of gases in the discharge zone.

Under such conditions, a strong effect of N_2 content on the temperature of gases was detected. When the laser device was operated continuously, the relationship between the temperature of working gases at the inlet and the N_2 content was measured, the result being shown in Fig. 6. With an increase in N_2 partial pressure, the temperature at the inlet in the discharge zone increased greatly; meanwhile, the working current of the axial flow blowing machine inside the laser device also increased remarkably.

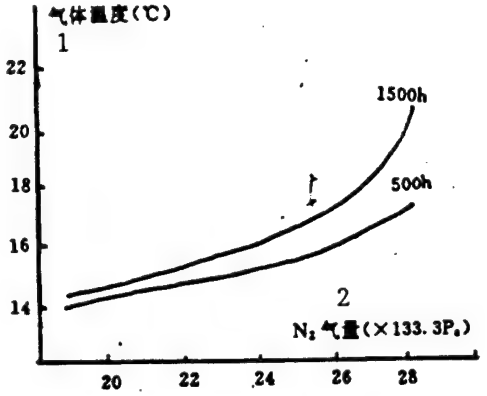

Fig. 6. Relationship of amount of N_2 gas and the temperature of the working ases
KEY: 1 - gas temperature 2 - amount of N_2 gas

This is because, given a constant total pressure of working gases, an increase in N_2 content will inevitably lead to a decrease in He, thus resulting in worse heat dissipation and in a temperature rise of the working gases.

In addition, by comparing temperature variation curves plotted at different operation periods, it was found that the temperature of working gases which operated 1500 hours appeared

higher than the temperature at the 500 hours level. This phenomenon was probably caused by the decrease in heat transfer efficiency due to scales formed in the heat exchanger by contaminating cooling water during the long-term operation of the laser device.

Conclusions

1. During long-term operation of the high power CO_2 laser device with a transverse gas flow system, its output power gradually decreases in stages in a stepwise manner.

2. With an increase in operating time of the high power CO_2 laser device with a transverse gas flow system, the total pressure of working gases must gradually be reduced so as to ensure the required laser output power level. Moreover, the total pressure of working gases has an optimal value in different device operating periods.

3. The CO_2:N_2:He distribution ratio must be adjusted at the same time as the total pressure of working gases is adjusted. To increase the N_2 partial pressure proportion in the working gases, the total pressure of working gases must be decreased. During different operating periods, there is an optimal value of the ratio between total pressure and partial pressure. At the same time, attention must be paid to the defect that the increase in N_2 content may lead to a temperature rise of working gases.

4. Adjusting the total pressure of working gases and gas distribution ratio proves to be an effective way of increasing laser device output power. It is helpful in increasing the longevity of the laser device and prolonging its operating time between overhauls.

REFERENCES

1. Run Yuwu et al., High Power Laser Processing and Applications, Tianjing Science and Technology Press, 1994, p. 1.

2. Cai Borong et al., Laser Devices, Hunan Science and Technology Press, Changsha, 1983, p. 8.

This paper was received on December 15, 1995.

NUMERICAL SIMULATION OF LASER IGNITION PROCESS

Sun Tongju, Shen Ruiqi, Dai Shizhi

College of Chemical Engineering,
Nanjing University of Science
and Technology, Nanjing 210094

ABSTRACT: A laser ignition model based on a thermal mechanism is developed in the paper. The model calculates the temperature history of laser ignition of $Mg/NaNO_3$. The calculation results agree with the experimental results and regularities.

KEY WORDS: laser ignition, numerical simulation.

Together with experimental studies of laser ignition devices, numerical simulation of the laser ignition characteristics of ignition devices also attracted widespread interest as a mathematical method of predicting the ignition characteristics of ignition devices during the irradiation of a laser. However, numerical simulation of an actual ignition process is
restricted[1-3] due to the swiftness and complexity of the interaction between the laser and the smoke and fire powder agents.

This paper presents the numerical simulation of the relationship between laser output parameters (energy level, beam diameter, pulse width) and the ignition characteristics of powder

agents; this relationship aimed at revealing some regularities in the ignition process.

Derivation of Mathematical Model

Like heater ignition, laser ignition is also a thermal process[1,3,4], which thereby can be described with heat flow energy balance equations, as follows:

$$\rho C\frac{\partial T}{\partial t}=K\left(\frac{\partial^2 T}{\partial x^2}+\frac{\partial^2 T}{\partial y^2}+\frac{\partial^2 T}{\partial z^2}\right)+H_1(T,t)+H_2(t) \tag{1}$$

$$H_1(T,t)=\rho Q\frac{\partial f}{\partial t},$$

$$\partial f/\partial t=(1-f)^n A\exp\left(-\frac{Ea}{RT}\right)$$

$$H_2(t)=(1-r)\beta I\alpha\exp(-\alpha z)$$

where ρ is density of powder agent ($kg\cdot m^{-3}$; C is heat capacity of the powder agent ($J\cdot kg^{-1}\cdot K^{-1}$); K is thermal conductivity of the powder agent ($W\cdot m^{-1}\cdot K^{-1}$); Q is chemical heat of reaction of the powder agent ($J\cdot kg^{-1}$); 1-f is reactivity of the powder agent; n is reaction series; A is frequency factor (S^{-1}): E_a is activation energy ($J\cdot mol^{-1}$); r is light reflectivity of the powder agent; β is light/heat conversion rate of the powder agent; I is incident laser intensity ($W\cdot m^{-2}$); α is light absorption coefficient of the powder agent (m^{-1}); z is thickness of the light-absorbing layer of the powder agent (m).

The laser energy obeys the Gaussian distribution, i.e.,

$$I(r,t)=I_0\exp(-r^2/r_0^2)\cdot\Phi(t) \tag{2}$$

where I(r,t) is laser energy distribution on the beam cross-section; r_0 is beam diameter (m); Φ is the waveform function $\int_{-\infty}^{+\infty}\Phi(t)=1$; I_0 is incident light intensity ($W\cdot m^{-2}$)

In solving this model, the following assumptions are introduced:

(1) The heat capacity and the heat conductivity of the powder agent are constants, i.e., their variation with temperature is ignored;

(2) The physical and chemical properties of the powder agent are distributed in axial symmetry and

(3) Decalescence of the powder agent is ignored.

Under cylindrical coordinates, Eq. (1) can be written as:

$$\rho C\frac{\partial T}{\partial t}=K\left(\frac{\partial^2 T}{\partial r^2}+\frac{1}{r}\frac{\partial T}{\partial r}+\frac{\partial^2 T}{\partial z^2}\right)+H_1(T,t)+H_2(t) \tag{3}$$

Eq. (3) is solved using the forward-differentiation format, i.e.,

$$T_{i,j}^{n+1}=T_{i,j}^{n}+A_{i,j}^{n}\Delta t,$$

$$A_{i,j}^{n}=K\left(\frac{T_{i+1,j}^{n}-2T_{i,j}^{n}+T_{i-1,j}^{n}}{\Delta r^2}+\frac{1}{r_{i,j}}\cdot\frac{T_{i+1,j}^{n}-T_{i-1,j}^{n}}{2\Delta r}+\frac{T_{i,j+1}^{n}-2T_{i,j}^{n}+T_{i,j-1}^{n}}{\Delta z^2}\right)+\frac{1}{\rho C}\left(H_{1i,j}^{n}+H_{2i,j}^{n}\right)$$

The condition for stabilizing the differentiation format is: $\Delta t\left(\frac{1}{\Delta r^2}+\frac{1}{\Delta z^2}\right)\leqslant 1/2$; the initial condition is $T(z,0)=T_0$; the boundary condition is that there must be thermal conductivity of gas and solid phases on the end face of the incident light, i.e., $T_s=T_g$, $-K_g\frac{\partial T_g}{\partial z}=-K_s\frac{\partial T_s}{\partial z}$; on other boundaries $A_{i,j}^{n}=0$.

Calculations

Prior to the numerical simulation of the ignition process of the powder agent under laser action, it is necessary to have advance knowledge of the thermodynamic properties of the powder

agent and its laser-absorbing character.

By using the parameters of the $Mg/NaNo_3$ powder agent proposed in reference[5] as well as by referring to the experimental results listed in the same reference, the authors examined the correctness of our established model and based on this examination, they explored the regularities occurring in the laser ignition process. For the physical and thermodynamic properties of the powder agent $Mg/NaNO_3$, see Table 1.

TABLE 1

Distribution ratio	58%Mg + 42%$NaNO_3$
Density ($kg \cdot m^{-3}$)	1650
Reflectivity	0.71
Heat capacity ($J \cdot kg^{-1}K^{-1}$)	1000
Thermal conductivity ($W \cdot m^{-1}K^{-1}$)	4.4
Absorptivity (m^{-1})	3.1×10^4
Frequency factor (S^{-1}	7.1×10^{17}
Activation energy ($J \cdot mol^{-1}$)	1.48×10^3
Heat of reaction ($J \cdot kg^{-1}$)	8.4×10^4

Assume the light/heat conversion rate β is 1, and that the reaction series is 2.

Fig. 1 shows the temperature rise under the same pulse width (200μs), the same beam diameter (0.8mm), and different energy levels of incident light.

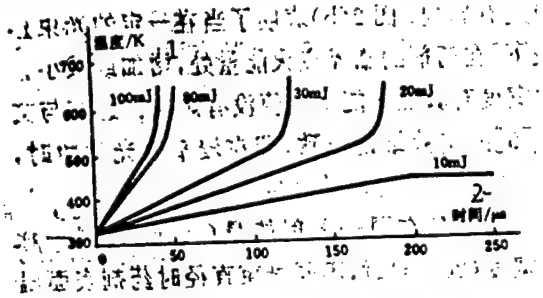

Fig. 1. Effect of incident energy level on the the surface temperature rise of the powder agent

Key: 1 - temperature 2 - time

It can be seen from Fig. 1 that the surface temperature rise of the powder agent accelerates with increase in the energy level of the incident light, i.e., the energy level of the incident light affects the ignition delay period. Furthermore, when the energy level of the incident light decreases to 10mJ, ignition will not take place. In this case, it can be determined that the critical ignition energy threshold of the powder agent given a beam diameter 0.8mm is approximately 10mJ, and the critical ignition energy density is around $2J/cm^2$. This result agrees closely with the experimental result presented in reference[5].

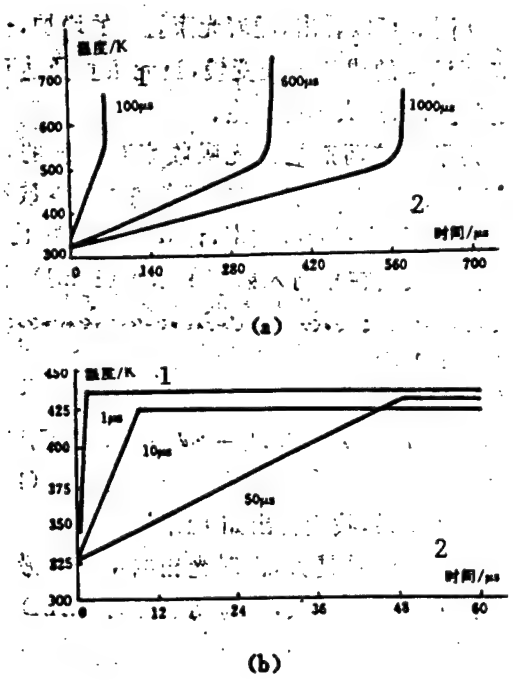

Fig. 2. Effect of pulse width on process of surface temperature rise of the powder agent
KEY: (a) 1 - temperature 2 - time
(b) 1 - temperature 2 - time

Fig. 2(a) shows the surface temperature rise of the powder agent given the same energy level of incident light (30mJ), the same beam diameter (0.8mm) but different pulse width, while (b)

shows the surface temperature rise of the powder agent given the critical ignition energy level (10mJ), the same beam diameter (0.8mm) but different pulse width.

Fig. 2(a) indicates that the surface temperature rise of the powder agent is prolonged as the pulse width is increased, i.e., the power of incident light has an effect on the ignition delay period. Fig. 2(b) suggests that given a certain beam diameter and the critical ignition energy of the powder agent, an increase or a decrease in pulse width has no effect on its ignition energy threshold. This also is in accord with the experimental results described in reference[5], i.e., with a narrower pulse, the ignition energy density is not related to pulse width.

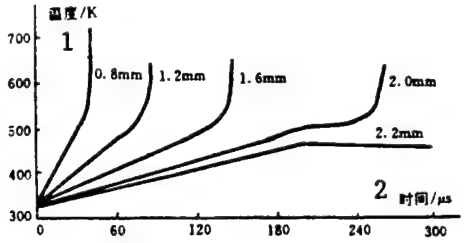

Fig. 3. Effect of beam diameter on surface temperature rise of powder agent
KEY: 1 - temperature 2 - time

Fig. 3 shows the surface temperature rise of the powder agent given the same incident energy (100mJ), the same pulse width (200μs) but different beam diameter.

It can be seen from Fig. 3 that the surface temperature rise of the powder agent slows down with increase in beam diameter, and when the beam diameter increases to a certain value, ignition will not take place.

To compare the effects of the laser absorption rate of the powder agent on sensitivity, its light absorption rate was

changed while other physical and thermodynamic parameters were held constant. The calculations are shown in Fig. 4.

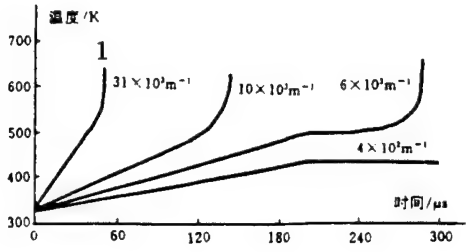

Fig. 4. Effect of light absorption rate on surface temperature rise of powder agent
KEY: 1 - temperature 2 - time

Fig. 4 indicates that given the same incident energy level (80mJ), the same pulse width (200μs), and the same beam diameter (0.8mm), the surface temperature rise of the powder agent is prolonged with decrease in the light absorption rate, and when it decreases to $4000m^{-1}$, ignition will not happen. This suggests that the ignition sensitivity of the powder agent decreases with decrease in light absorption rate.

Conclusions

The results of the foregoing tentative numerical simulation show that the mathematical model that we derived and its solution are basically correct. Through numerical calculations of the surface temperature rise of the powder agent given various parameters, some results of significance were obtained, which can lead us to a deeper understanding of certain regularities occurring in the laser ignition process. Nonetheless, the model-based calculations of the ignition delay period are yet experimentally supported.

REFERENCES

1. Ewick, D.W., 15th IPS, 1990, 7, P277.

2. Skocypec, R.D. et al., 15th IPS, 1990, 7, P877.

3. Ewick, D.W., 18th IPS, 1992, 7, P255.

4. Glass, M.W. et al., 18th IPS, 1992, 7, P321.

5. Ostmark H. et al., J. Appl Phys., 1993, 73(4), 1193

This paper was received on December 27, 1995.

ANALYTICAL SOLUTION OF SHORT-CAVITY DYE LASER

Lu Bingsong, Wang Zhongjie

Physics Department
Anhui Normal University
Wuhu 241000

ABSTRACT: The pulse shape of a dye laser and formula of pulse duration of a dye laser were obtained by solving rate equations. The value that was calculated using this approximation formula of pulse duration was close to that found by solving the rate equations by computer.
KEY WORDS: short-cavity dye laser, rate equations, pulse duration.

Through the transient response of control cavities, a short-cavity dye laser can derive pulse compression. Such a phenomenon occurring in short-cavity dye lasers (SCDL) was observed and studied by numerous researchers[1,2]. They pointed out that narrow and giant single pulses can be obtained if the pumping rate is properly controlled so that the SCDL can operate above the threshold, and so that rate equations can be used for better description of the time domain behavior of the SCDL.

Reference[3] presents a formula for calculating the pulse duration of the dye laser, which was derived through a segmented approximation solution to rate equations. Reference[4] provides

an approximation formula for calculating pulse duration with a pump slightly higher than the threshold.

Further efforts were made in this paper in this field. Similarly, we obtained, through appropriate approximation of rate equations, not only the formula for calculating the pulse duration of a dye laser, but also a formula for calculating its pulse time domain.

Rate Equations and Analytical Solution

It is well known that a set of rate equations can be used to describe the time domain behavior of a short-cavity dye laser. In this case, the laser is regarded as an ideal four-level system, and the effect of triplet on singlet is ignored. During single-mode operation, the rate equations are:

$$dn/dt = R(t) - Bnq - n/\tau_f \tag{1}$$

$$dq/dt = Bnq - q/\tau_c + f \cdot n/\tau_f \tag{2}$$

where n and q, respectively, are the density of the in-cavity inversion population and the density of photon number; R(t) is pumping rate; τ_f is fluorescence lifetime; B is Einstein coefficient; τ_c is lifetime of in-cavity photons; and f is percentage of fluorescence transmitted in the laser direction.

As soon as the pump operates, the SCDL causes an inversion of the population and greatly exceeds the threshold. When the dye laser pulses have been generated, the pumped light rate and self-radiation can be ignored compared with the larger density of the photon number of dye laser pulses. At this instant, the SCDL operates near the threshold. Thus, during the generation of dye laser pulses, Eqs. (1) and (2) can be simplified as follows:

$$dn/dt = - Bnq \tag{3}$$

$$dq/dt = Bnq - q/\tau_c \tag{4}$$

By integrating Eq. (3) and defining $I(t) = \int_0^t q(t)dt$,

$$n = n_0 e^{-BI(t)} \tag{5}$$

where n_0 is the density of the inversion population when the dye laser pulses have yet to be generated. By substituting Eq. (5) in (4) and then integrating, the following can be derived:

$$dI/dt = q_0 - n_0 e^{-BI(t)} + n_0 - I(t)/\tau_c \tag{6}$$

where q_0 is the density of the self-radiated photon number when the dye laser pulses have not yet been generated.

Since the density of the in-cavity inversion population remains near the threshold, $n(t) \sim n_t$ (n_t is density of the inversion population of the threshold), while $n_t << n_0$, and therefore, $BI(t) << 1$. In Eq. (6), $e^{-BI(t)}$ can be expanded into a power series while ignoring power terms that are higher than the second one. By doing so, Eq. (6) becomes

$$dI/dt = q_0 + (n_0 B - \frac{1}{\tau_c})I - \frac{1}{2}n_0 B^2 I^2 \tag{7}$$

The foregoing differential equation is a Riccati equation. Then by introducing the density of the inversion population of the threshold $n_t = 1/B\tau_c$, and letting $\alpha = \frac{1}{2}(n_0 B - \frac{1}{\tau_c}) = \frac{1}{2}B(n_0 - n_t), \beta = \frac{1}{2}n_0 B$, Eq. (7) will become

$$dI/dt = q_0 + 2\alpha I - B\beta I^2 \tag{8}$$

The solution to this equation is

$$I(t) = q_0 \frac{1 - e^{-2rt}}{r_1 + r_2 e^{-2rt}} \tag{9}$$

where

$$r = (\alpha^2 + \beta B q_0)^{1/2} \approx \alpha \tag{10}$$

(q_0 is usually very small)

$$r_1 = r - \alpha \approx \beta B q_0 / 2\alpha \tag{11}$$

$$r_2 = r + \alpha \approx 2\alpha \tag{12}$$

Again by differentiating Eq. (9), the density of the photon number of the dye laser pulses q(t) can be derived as

$$q(t) = q_m \operatorname{sech}^2[r(t - t_m)] \tag{13}$$

where $q_m = \frac{r^2}{B\beta} \approx \frac{1}{2} n_0 (1 - \frac{n_t}{n_0})^2$ is the density of peak photon number.

$$t_m = \frac{ln(r_2/r_1)}{2r} \approx \frac{ln[2n_0(1 - \frac{n_t}{n_0})^2/B^2 q_0]}{B(n_0 - n_t)}$$

It can be seen from Eq. (13) that the dye laser pulses are in the form of arc waves as shown in Fig. 1. Also, from Eq. (13), it is easy to calculate the total width of the semi-maximum value of the dye laser pulse as

$$t_p = (2/r) \cdot ln(1 + \sqrt{2}) \approx 1.767/r \approx 3.5\tau_c/(\frac{n_0}{n_t} - 1) \ (FWHM) \tag{14}$$

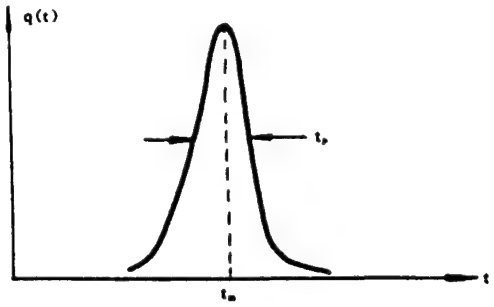

Fig. 1. Shape of dye laser pulse

Results and Discussion

Based on the data provided in reference[5]: dye: rhodamine 6G; concentration 3 x 10^{-3} mol·l^{-1}; lifetime of in-cavity photon number τ_c=19.1PS; lifetime of fluorescence τ_f=5ns; pumped beam: λ_p=337.1nm N_2 laser beam and pulse duration T_1=2nS, we selected double pumped pulse duration as the effective pumping time T_c=4ns. The value of n_0 can be calculated in the following way: when Eq. (1) ignores the excited transmission (because the dye laser has not been generated when pumping starts),

$$dn/dt = R(t) - n/\tau_f \tag{15}$$

By solving Eq. (15),

$$n_0 = R\tau_f(1 - e^{-w/\tau_f}) \tag{16}$$

where t_c is time interval between the start of pumping and the start of generation of the dye laser, and $t_0=T_c/2+t_d$, t_d is the relative delay value of the output light pulse to the pumped light pulse; the experimental value of t_d is 1.3ns according to reference[5], so t_0=3.3ns. Taking the total pumped photon number

$$\mathcal{N} = \int_0^\infty R dt \approx R \cdot T_c$$

into account, Eq. (16) is converted to

$$n_0 = \frac{\mathcal{N}}{T_c} \cdot \tau_f (1 - e^{-t_0/\tau_f}) \qquad (17)$$

By inserting the t_0 value in the above formula, we calculated $n_0 = 0.48\mathcal{N}$.

When $\mathcal{N}/n_t = 4.99$, by taking $n_0 = 0.48\mathcal{N}$ into account, t_p=48PS can be obtained, which agrees with the numerical calculations in reference[5] (47PS).

It can be seen from Eq. (14) that by shortening the cavity length L, i.e., by reducing τ_c ($\tau_c=\eta L/c(1-R)$, where η is the dye refractivity, and R is the refractivity of the cavity), extremely narrow dye laser pulses can be derived. Similarly, by increasing n_0/n_t, i.e. by increasing the pumping rate, and decreasing the threshold of the laser, a narrow light pulse output can also be obtained. In addition, it can also be seen from Eq. (10) that q_0 has an indistinct effect on the pulse duration of the dye laser.

REFERENCES

1. Roess, D., J. Appl. Phys., 1966, 37, 2004
2. Lin, C. et al., Appl. Phys. Lett., 1975, 26, 389
3. Wenju Chen, Optics Journal, 1983, 3, 805
4. Zhongjie Wang, Rev. Roum. Phys., 1989, 34, 891
5. Amada, K. Y. et al., Appl. Opt., 1986, 25, 634

This paper was received on January 7, 1996.

METHOD OF MEASURING REFLECTIVITY OF ULTRA-LOW-LOSS MIRROR COATINGS

Jiang Yue, Chen Jiansong

Air Force Radar Academy
Wuhan 430010

ABSTRACT: This paper introduces a method of measuring the ultra-high reflectivity of laser mirrors by measuring the intensity decay time of an optical cavity, and the resolution can measure up to~10^{-6} of reflectivity of ultra-low-loss mirror coatings.

KEY WORDS: optical cavity, ultra low-loss, ultra-high reflectivity, decay time

Ultra-low-loss mirror coatings are vital in high precision optical instruments, including laser gyros. This paper proposes a method for measuring the refractivity of ultra-low-loss mirror coatings by measuring the decay time of passive resonant cavities.

Principles of Measurement

The device that we introduce in this paper serves in measuring the decay time of light radiation in passive resonant cavities τ_R, which can be converted into the total losses of the resonant cavity, and δ, the refractivity of its cavity mirror R.

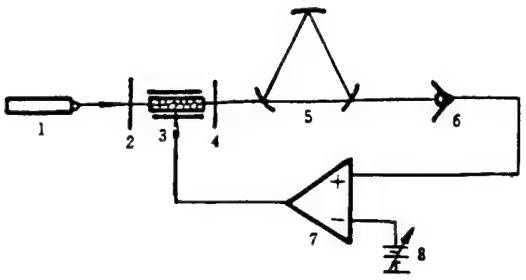

Fig. 1. Principles of decay time measurement
KEY: 1 - laser 2,4 - polarizing filters
3 - electrooptic crystal 5 - passive resonant cavity 6 - detector
7 - comparator 8 - reference voltage

As shown in Fig. 1, once the incident laser beam arrives at the resonant cavity to be measured and attains resonance, the light intensity in the passive cavity will be subjected to exponential decay when the incident light source is cut off. The decay time is determined by the total cavity losses and length, unrelated to incident light intensity. Here, we briefly discuss how to derive the formula for calculating decay time τ_R, and the relationship between the reflectivity of the cavity mirror and the cavity loss, given small losses.

The average one-way loss factor $\delta(\delta')$ can be defined using the following formula:

$$I_1=\begin{cases} I_0 e^{-2\delta} & \text{(straight cavity)} \\ I_0 e^{-\delta'} & \text{(ring cavity)} \end{cases} \qquad (1)$$

where I_0 is the initial light intensity; I_1 is the light intensity after a return trip within the passive cavity. If the losses are caused by multiple factors, then the corresponding loss factor is δ_i,

$$I_1=I_0 e^{-2\delta_1}\cdot e^{-2\delta_2}\cdots e^{-2\delta_n}=I_0 e^{-2\delta} \qquad (2)$$

The total loss can be expressed as

$$\delta=\sum_{i=1}^{n}\delta_i=\delta_1+\delta_2+\cdots+\delta_n \qquad (3)$$

From Eq. (1), it can be calculated that after a m number of return trips, the light intensity will be

$$I_m = I_0(e^{-2\delta})^m = I_0 e^{-2m\delta} \quad \text{(straight cavity)}$$
$$I_m = I_0(e^{-\delta'})^m = I_0 e^{-m\delta'} \quad \text{(ring cavity)} \qquad (4)$$

If the light intensity at t=0 is selected as I_0, then by the time t, the number of return trips of the light within the cavity m should be:

$$m = \begin{cases} \dfrac{t}{2L/C}, & \text{(straight cavity)} \\ \dfrac{t}{L/C}, & \text{(ring cavity)} \end{cases} \qquad (5)$$

where L is the optical length of cavity; C is the speed of light in vacuo.

The light intensity at t can be calculated by substituting Eq. (5) in (4):

$$I(t) = I_0 \exp(-\frac{t}{\tau_R}) \qquad (6)$$

where

$$\tau_R = L/\delta C \qquad (7)$$

i.e., the decay time constant of light radiation in the passive resonant cavity.

It is known from Eq. (7) that the losses of the cavity to be measured $\delta(\delta')$ can be derived as long as the cavity length L and the decay time τ_R have been measured.

If the resonant cavity is made up of n lenses with R_i as the reflectivity of the i-th lens, and α_i as its total loss, then

$$|R = \prod_{i=1}^{n} R_i = \prod_{i=1}^{n} e^{-\alpha_i} \quad \text{(straight cavity)}$$
$$= e^{-\sum_{i=1}^{n}\alpha_i} = \begin{cases} e^{-2\delta} & \text{(ring cavity)} \\ e^{-\delta'} & \end{cases} \qquad (8)$$

For ultra-low-losses, $e^{-\alpha_i} \approx 1-\alpha_i$, $R_i = 1-\alpha_i$

In this way, the direct relationship between the product of mirror reflectivity $|R$ and the cavity losses $\delta(\delta')$, assuming ultra-low losses, can be calculated as follows:

$$|R=\prod_{i=1}^{n}R_i\cong\begin{cases}(1-\frac{2\delta}{n})^n\cong 1-2\delta & \text{(straight cavity)}\\ (1-\frac{\delta'}{n})^n\cong 1-\delta' & \text{(ring cavity)}\end{cases} \quad (9)$$

It is known from Eq. (9) that if all the mirror reflectivities of the cavity to be measured are unknown, it is possible to first produce a (n+1) number of different combinations (using n mirrors each time) by applying (n+1) mirrors. In this case, the reflectivity of a single lens can be calculated as long as the same $|R$ value is measured each time. Once scaled, the follow-up test items need only one measurement and replacement of one known mirror. Obviously, it is the easiest way to use straight cavities for scaling. However, actually we used ring cavities instead because we considered the real structure of gyros.

Experimental Device

Fig. 2 is a simple diagram of an experimental device. The process of its operation is: If the frequency of the incident laser beams coincides with the resonant frequency of the passive cavity, then it will be intensified through resonance and will emit from the cavity, and the light intensity of the output mirror will be received by a detector. When the intensity of the emitted light reaches the preset threshold level of a comparator, then the comparator will, through the output, trigger the field-effect transistor flow, and impose a semi-wave voltage to an electrooptical crystal to cut off the laser beam that has entered the cavity. Furthermore, the detector is used to monitor the light decay level, and a timer (or a digital memory oscillograph) is used to measure the time spent from intensity decay to intensity 1/e upon the cut-off, i.e., τ_R.

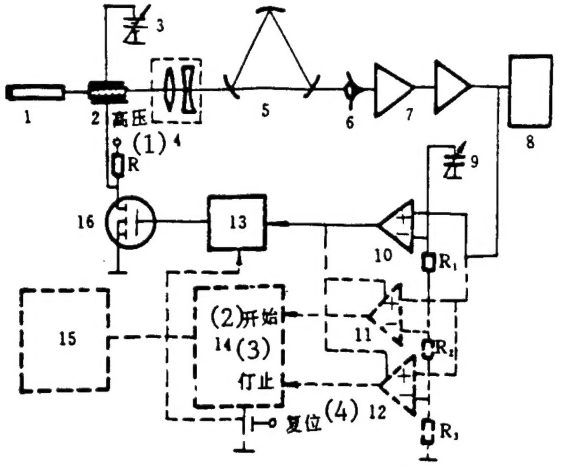

(R_1, R_2, R_3 must satisfy the following:)

$$\frac{R_2+R_3}{R_1+R_2+R_3}\leqslant 1;\ \frac{R_3}{R_2+R_3}=\frac{1}{e})$$

Fig. 2. Experimental device
KEY: (1) - high pressure (2) - start
(3) - end (4) - reset

1 - source laser 2 - electrooptical switch 3 - offset power supply 4 - standard matched lens set 5 - passive resonant cavity to be measured 6 - photoelectric detector 7 - prepositioned low-noise and broadband amplifier 8 - digital memory oscillograph 9 - reference power supply 10, 11, 12 - comparators 13 - double stable trigger 14 - digital timer 15 - display (oscillograph) 16 - switching tube (MOSFET)

Measurement Accuracy

To find the proper requirements for the response speed of the electronics system so as to select appropriate components, we list the ultimate measurement accuracy that our device can attrain in the following table (under the assumption that the timing accuracy τ=0.60μs, length of straight cavity l=1m, and R is mirror reflectivity).

TABLE 1. Measurement Accuracy (Theoretically Estimated Values)

$R_1=R_2$	腔损耗 δ(%) 1	衰减时间 τ_R(μs) 2	$\frac{\Delta\tau_R}{\tau_R}(\frac{\Delta\delta}{\delta})$(%)	分辨率 Δδ 3 (×10⁻⁴)
0.999000	0.10	3.33	18	±180
0.999900	0.010	33.3	1.8	±1.8
0.999990	0.0010	333	0.18	±0.18

KEY: 1 - cavity loss 2 - decay time 3 - resolution

The above table shows that as long as the timing accuracy is better than 0.60μs, the measurement accuracy can exceed 0.00018% for cavities with losses less than 0.10%, although the accuracy can be only 0.018% when cavity losses are 0.010%. Therefore, this device can reach an ultra-high measurement accuracy that is better than $\pm 2.000000 \times 10^{-6}$ for cavity mirrors with reflectivity R less than or approximately equal to 0.99990 as long as the fall time of individual components is less than or equal to 100ns, and the sum of the fall time of the entire system is less than or equal to 600ns.

The measurement accuracy of our method basically depends on the loss of the resonant cavity: the lower the cavity loss, the higher the measurement accuracy can be. While other methods, otherwise, suffer from a common defect, that is: the lower the loss, the larger the error can be, and therefore, they are incapable of measuring ultra-low losses. Technically, this decay time measurement method can not only overcome the foregoing defect, but also change the defect into a condition for raising the measurement accuracy.

This paper was received on January 7, 1996.